Pramāṇa – J. Phys., Vol. 30, No..6, June 1988, pp. 569–595. © Printed in India.

Measurement and understanding of magnetization in AC and DC fields and the determination of intragrain H_{c1} in high T_c $RBa_2Cu_3O_7$ superconductors

A K GROVER, C RADHAKRISHNAMURTY†, P CHADDAH*, G RAVI KUMAR* and G V SUBBA RAO**

Tata Institute of Fundamental Research, Bombay 400 085, India
*Bhabha Atomic Research Centre, Bombay 400 085, India
**Indian Institute of Technology, Madras 600 036, India

MS received 5 April 1988

Abstract. We present DC and low frequency AC magnetization measurements on various $RBa_2Cu_3O_7$ superconductors. We identify features intrinsic to these compounds, and establish the features originating from intergranular links in sintered pellets. The isothermal magnetization curves, and the temperature dependence of magnetization in field-cooled and zero field-cooled states are shown to be consistent with the calculations done following a recent extension of Bean's model. Low field anomalies predicted within this model are observed, and yield H_{c1} values of a few Oe. These values are shown to be consistent with the temperature variation of magnetization. A comparison is made with the other existing data and it is demonstrated that earlier quoted values of H_{c1} are gross overestimates.

Keywords. High temperature superconductors; lower critical field; magnetization curves; critical currents; AC methods; DC methods; hysteresis loops.

PACS Nos 74·30; 74·60

1. Introduction

The lower critical field H_{c1} is a basic physical parameter of a type II superconductor and its value can be used to infer microscopic properties of the superconducting state. The textbook definition of H_{c1} is the field below which there is a complete flux expulsion. When a magnetization measurement is made on a sample of macroscopic size, macroscopic shielding currents can be set up at $H > H_{c1}$ which will effectively shield the bulk of the sample from the magnetic field (Bean 1962, 1964). It is the experimentalist's problem to find ways to distinguish this macroscopic shielding (which, though not ideally total, may appear total within the experimental error) from the thermodynamic Meissner state and thus determine H_{c1}.

The magnetization measurements are usually made to obtain information about the extent of magnetic flux expulsion in superconductors. The magnetization curve of a superconducting sample is obtained by first cooling the sample to a given temperature in zero field (ZFC) and then gradually raising the externally applied field H_e. Upto the field H_{c1} (ignoring the demagnetization correction) the screening currents are set up at

†To whom all correspondence should be addressed.

the sample surface to within the London penetration depth and the sample exhibits perfect diamagnetism with its magnetization proportional to H_e. As H_e is raised above H_{c1}, the macroscopic shielding currents start to flow in the sample (Bean 1962, 1964). The resulting magnetization of the specimen, to zeroth order, is that of a perfect diamagnet even above H_{c1}. The first order term accounting for deviation from perfect diamagnetism is proportional to H_e/H^*, where H^* is a parametric field which is directly related to the macroscopic current density and the dimensions of the superconducting grain. This implies that if the magnetization is measured to a fractional accuracy of x, then the flux expulsion may appear complete upto $H_e < xH^*$. Therefore, the conventional way of defining H_{c1} as the point where M vs H_e curve deviates from linearity becomes suspect for samples with very large H^* values (compared to H_{c1}), such as high T_c oxide superconductors. It was recently pointed out by Ravi Kumar and Chaddah (1987) that instead of using the virgin magnetization curve, H_{c1} may be determined from the hysteretic part of the magnetization curve where it manifests as an anomaly in the region $H_e < H_{c1}$.

The anomalies near $H_e = 0$ in the magnetic hysteresis data of high T_c materials have been reported by various workers (Schneemeyer *et al* 1987; Senoussi *et al* 1987a; Grover 1988). These indicate H_{c1} values for oxide superconductors to be very much lower (see, for instance, Grover 1988) than those at which M vs H_e curves deviate from linearity during the respective virgin runs. We report in this paper the results of systematic investigations on a variety of superconducting $RBa_2Cu_3O_7$ specimens using DC and AC magnetization methods. We compare our observations with the existing data in literature. There has been some apparent confusion originating from the results of investigations on polycrystalline (see e.g. Maletta *et al* 1987; Renker *et al* 1987; Rosenberg *et al* 1987; Senoussi *et al* 1987b, c; Marcus *et al* 1987; Grover *et al* 1988; Grover 1988; Wiesniewski *et al* 1988) and single crystal specimens (Senoussi *et al* 1987a; Schneemeyer *et al* 1987; Umezawa *et al* 1987a, b; Gammel *et al* 1987; Hammann *et al* 1987) of oxide superconductors. The results presented in this paper unambiguously clarify the situation. We are able to distinguish between anomalies in magnetic hysteresis data arising from the intragrain (intrinsic) and intergrain regions of high T_c oxides. We confirm that H_{c1} values in these high T_c compounds are indeed low. We find that almost all the key magnetization results reported so far can be qualitatively explained in terms of calculations based on an extension (Ravi Kumar and Chaddah 1987) of Bean's original model (1962).

2. Experimental

2.1 *Samples*

The samples investigated belong to $RBa_2Cu_3O_7$ family. Measurements have been made on different specimens of compounds with R = Y, Gd, Ho, Dy, Tb and $Y_{0.8}R'_{0.2}$ (with R' = Lu, Gd, Ho, Yb and Dy). Most of these specimens were synthesized following the same recipe (Subba Rao *et al* 1987). A few of the Y specimens were, however, synthesized following a slightly different heat treatment to crosscheck the observed magnetic behaviour by AC measurements. All the specimens were single-phased with zero resistance state being attained at above 90 K.

2.2 *DC measurements*

The magnetization curves in steady magnetic field were obtained using the Faraday method. The magnetic field was produced by an electromagnet and the gradient field was obtained by a pair of Lewis coils. The experimental set up used was such that the DC magnetic field could be varied without interruption from -50 to 8000 Oe. The field could not be changed in steps smaller than about 1·6 Oe. The magnetic force on the sample is in the direction normal to the direction of the DC field due to the electromagnet. The field gradient was limited to a value of 12 Oe/cm. The applied magnetic field values were read using a Hall probe placed outside the cryostat. Using a strongly magnetic sample, it was ensured that the Hall probe is so located that it faithfully measures the field at the sample position. We estimate a systematic error of less than 3 Oe in our absolute field values, whereas the relative error in different field values is about 0·2 Oe. The pellet specimen had the dimensions $6{\cdot}5 \times 2{\cdot}2 \times 2{\cdot}2\,\text{mm}^3$ whereas the powder specimen was put inside a copper bucket with internal diameter of 4 mm. Considering the finite dimensions of the specimens, we have measured the magnetization with a resolution function of FWHM < 2 Oe. The gradient field was switched on only while recording the magnetic force at a fixed field value. The force value was recorded about a minute after switching on the gradient field. The force with the gradient field in the reversed direction was not recorded to avoid any possible complications because of hysteresis. The magnetic isotherms were measured at 77 K and 5 K; at these temperatures it was possible to ensure the stability of the sample temperature over long times.

The DC magnetization data were recorded only on one compound, namely, $Lu_{0{\cdot}2}Y_{0{\cdot}8}Ba_2Cu_3O_7$, both in its sintered pellet as well as crushed powder forms. Most of these data are presented in figures 1 to 8. The arrows in figures 1 to 7 indicate the direction in which the field was varied and the different magnetization curves are identified by the number of the field cycle. The dotted lines through the data points are only a guide to the eye. The measurements made on the pellet and powder specimens include the following:

(i) M vs H_e curves at 77 K in pellet (figure 1a) and powder (figure 6a) on their zero field-cooled states in field values upto 1500 Oe. The minor hysteresis loops were recorded in field values of ± 45 Oe and ± 10 Oe in pellet (figure 1b) and powder (figures 6b and c) specimens respectively after reversing the field from -50 Oe.

(ii) M vs H_e curves at 77 K on pellet (figures 2a and b) and powder (figure 7) in fields upto ± 10 Oe.

(iii) M vs H_e curves at 77 K and 5 K on pellet in fields of ± 45 Oe (see figures 3 and 5 respectively).

(iv) M vs H_e curve at 5 K on ZFC pellet in field upto 6 kOe (figure 4a). Figure 4b shows the hysteretic behaviour near $H_e = 0$ on an expanded scale.

(v) Magnetization vs temperature behaviour on the pellet from 20 K to 95 K in a nominal field of 10 Oe in both the nominal zero field-cooled and field-cooled states (figure 8). In the first case, the sample was cooled down to about 20 K in nominal zero field and magnetization was then measured in a field of 10 Oe during the warm-up cycle. The DC field was kept on during the warm-up whereas the gradient field was switched on only while recording the force value at selected temperatures. The

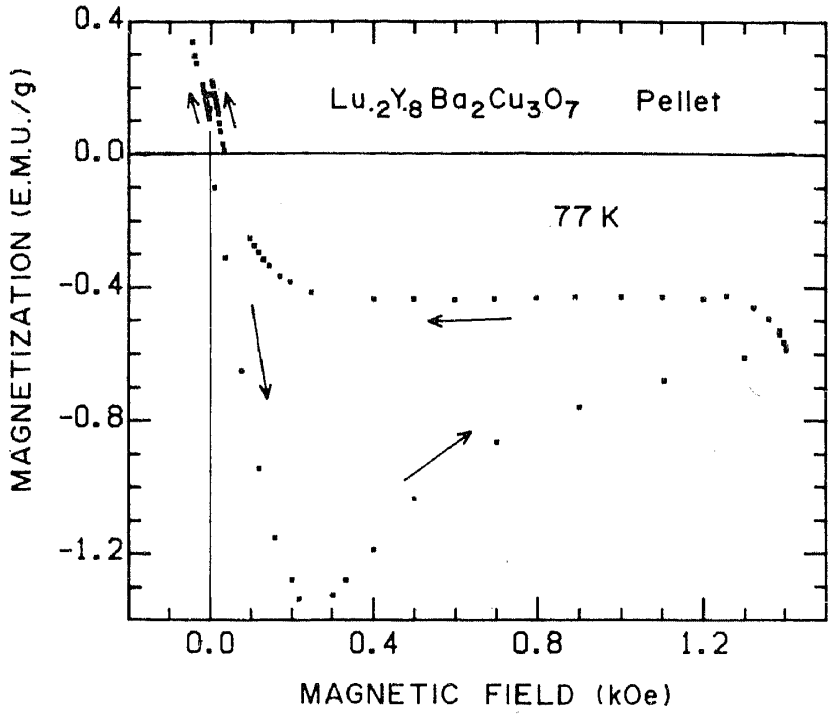

Figure 1a. Magnetic hysteresis curve at 77 K for a sintered pellet of $Lu_{0.2}Y_{0.8}Ba_2Cu_3O_7$ in DC field upto 1500 Oe. The specimen was cooled down to 77 K in nominal zero field. The arrows indicate the direction in which the field was varied. The anomalous dip in magnetization values near zero field value on the reverse cycle is sandwiched between the pair of arrows.

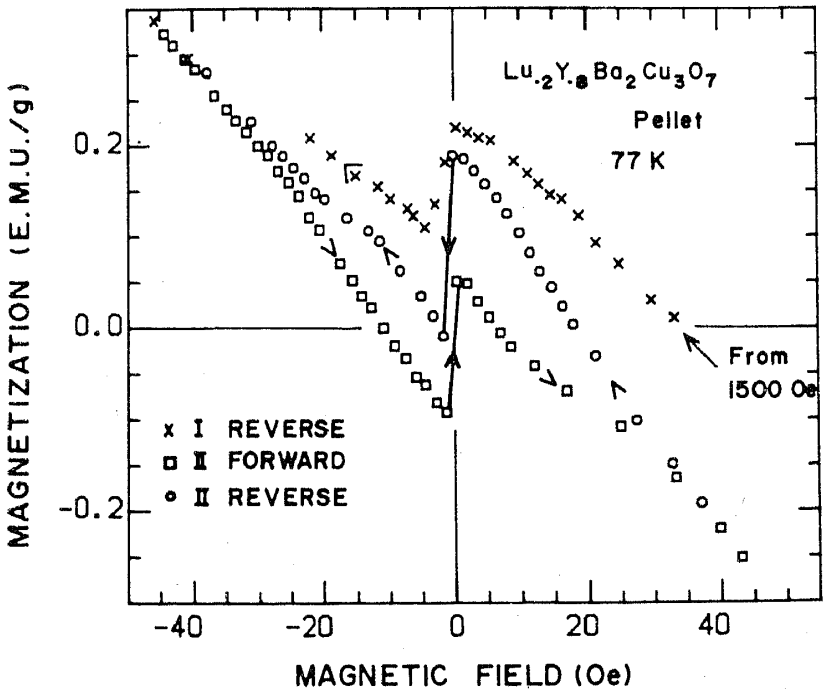

Figure 1b. Magnetic hysteresis curves for the pellet specimen of $Lu_{0.2}$ at 77 K on repeated cycling between $\pm$ 45 Oe. The specimen was first exposed to a field of 1500 Oe. The anomalous dip of figure 1a can be clearly identified on the I reverse cycle.

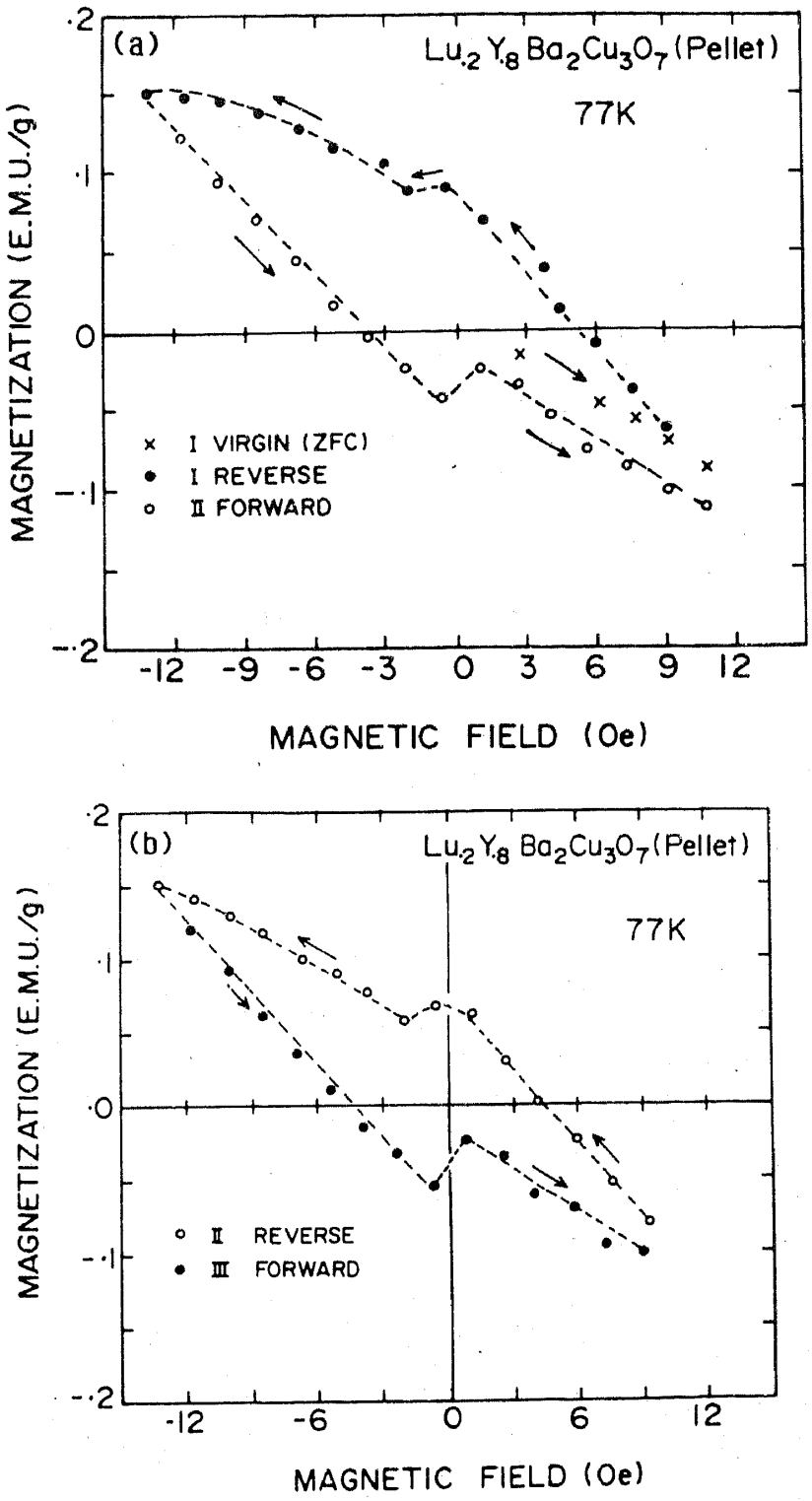

Figure 2. **a** and **b**. Minor hysteresis loop obtained in DC field of ± 10 Oe at 77K for the sintered pellet of $Lu_{0.2}Y_{0.8}Ba_2Cu_3O_7$. The anomalous dip near zero field values can be identified in the loops.

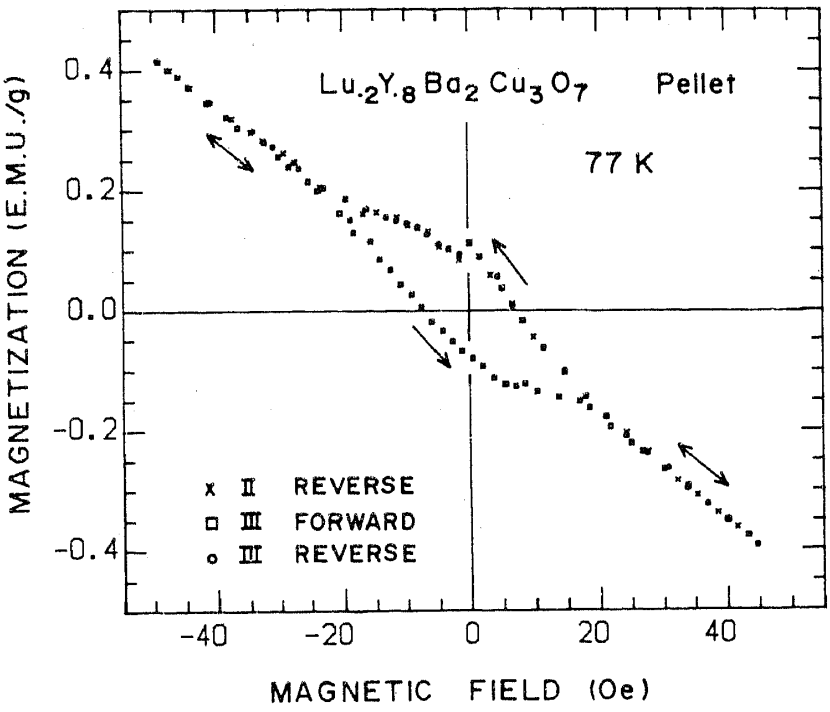

Figure 3. Minor hysteresis loop obtained at 77 K for the pellet specimen of $Lu_{0\cdot2}$ after repeated cyclings in a DC field of ± 45 Oe.

continuous lines shown in figure 8 are the smooth curves drawn through discrete data points.

2.3 *AC measurements*

The AC magnetization measurements give information about the steady state response of specimens at a given frequency. These measurements were performed using low (Likhite and Radhakrishnamurty 1966) and high (Radhakrishnamurty *et al* 1971) field techniques developed initially for the quick study of the superparamagnetic aspects of rock samples. Due to the ease with which data could be obtained on these instruments, we studied the AC magnetic hysteresis of all the sintered pellet specimens. Several of the specimens were also studied in their powder form. For brevity, we show only some of the representative data in figures 9 to 12. The measurements made on different specimens can be listed as follows:

(a) Study of hysteresis loops at 77 K in fields below and up to 20 Oe at a frequency of 317 Hz. From these data, a comparative study could be made about the extent of irreversibility at low field values in different specimens. They also provide a measure of the lowest field values in which irreversibility can be seen (within the sensitivity limit of the instruments used) in different specimens and in different orientations of each specimen.

(b) Record of hysteresis loops at 77 K in peak fields ranging from 30 to 1500 Oe at a frequency of 50 Hz. These data vividly show the changes in shape of the magnetic hysteresis curves as peak field gradually increases.

(c) Temperature variation of AC susceptibility from 20 to 300 K in different peak fields.

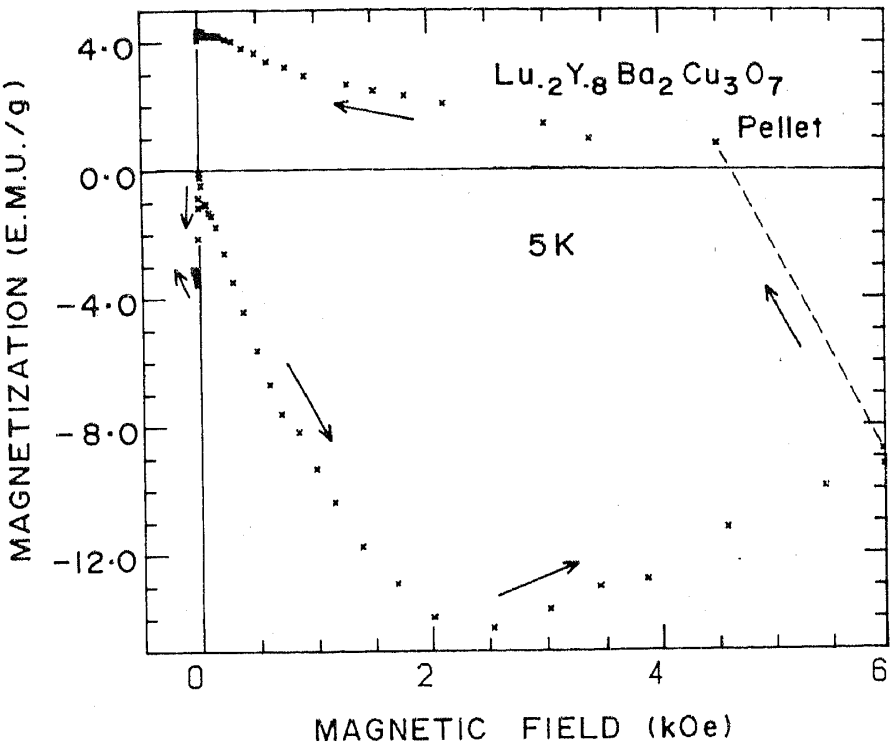

Figure 4a. Magnetic hysteresis curve at 5 K for the pellet of $Lu_{0.2}$ in a DC field upto 6 kOe. The specimen was zero field-cooled to 5 K and the arrows indicate the direction in which the field was varied. The sharp drop in magnetization near zero field value on the first reverse cycle can be identified by following the arrows.

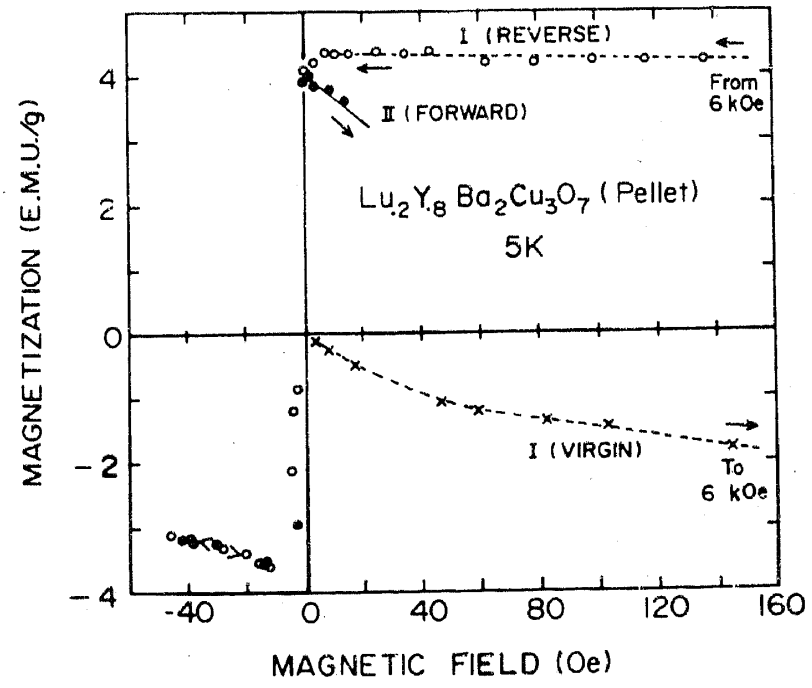

Figure 4b. Magnetization vs field curve at 5 K on reversal of field from -45 to $+20$ Oe in $Lu_{0.2}$ specimen (II forward). The initial virgin and a part of the first reverse cycle curves shown in figure 4a have also been plotted on an expanded scale.

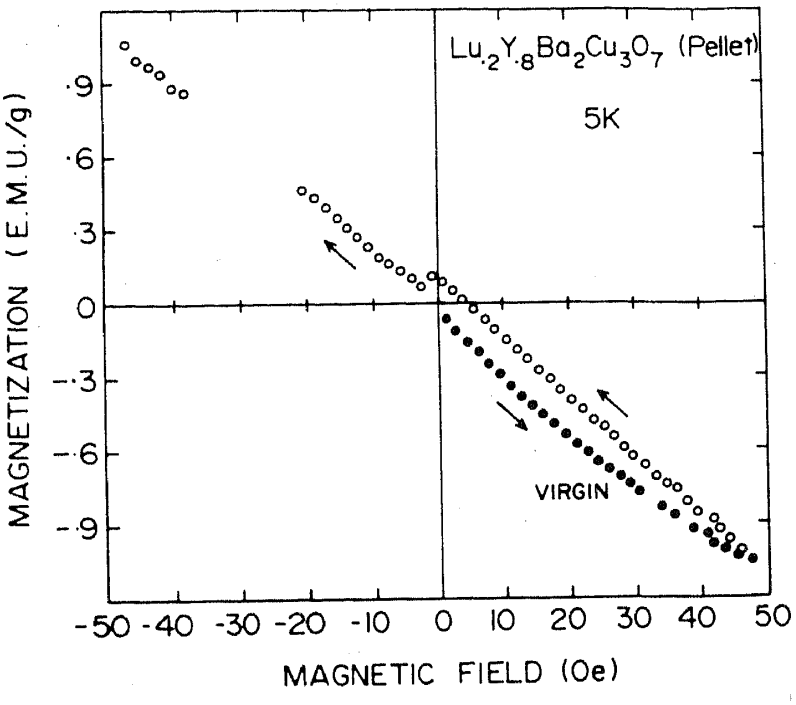

Figure 5. Magnetic hysteresis curve at 5 K for the pellet of $Lu_{0\cdot2}$ in $\pm$ 45 Oe. The small dip in magnetization near zero field value on the reverse cycle can be identified.

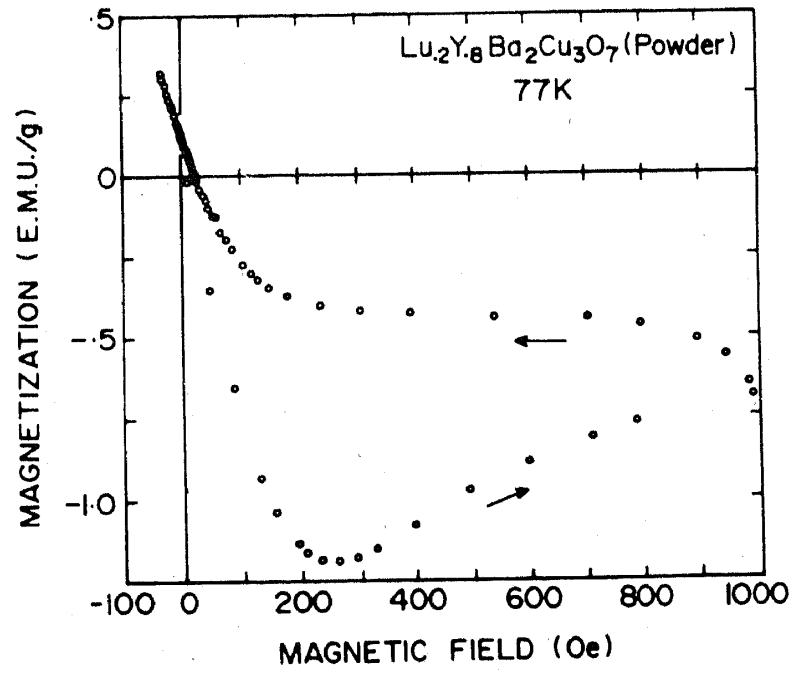

Figure 6a. Magnetic hysteresis curve at 77 K for powdered specimen of $Lu_{0\cdot2}$ in DC field upto 1 kOe. The sample was cooled down first in nominal zero field, the arrows indicate the direction in which the field was varied.

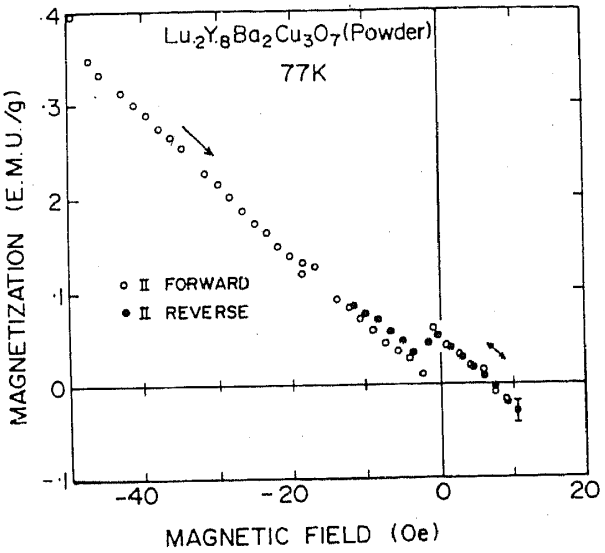

Figure 6b. Magnetic hysteresis curves in ± 10 Oe on reversal of field from -45 Oe for powdered specimen of $Lu_{0\cdot2}$ at 77 K.

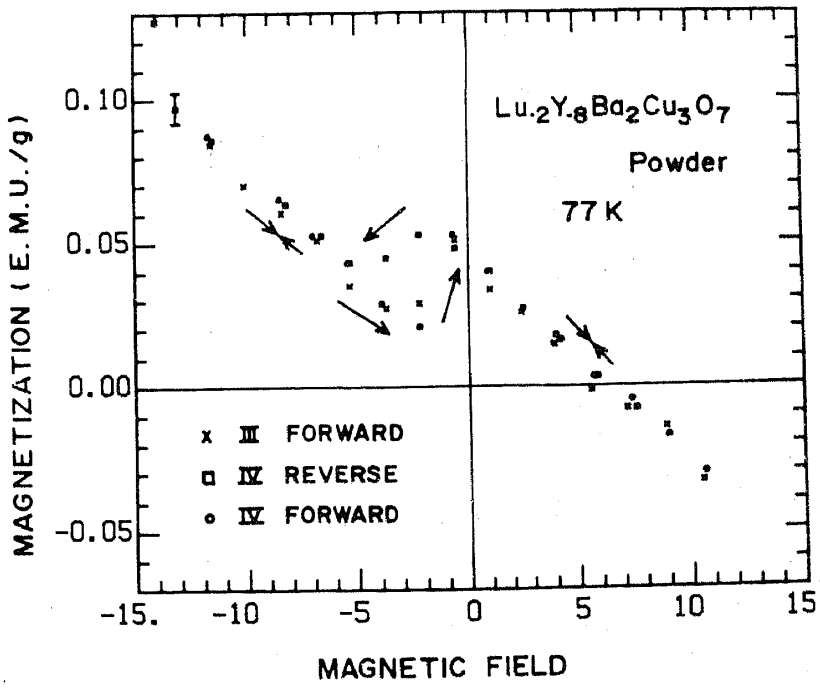

Figure 6c. Magnetic hysteresis loop on repeated cycling between ± 10 Oe for $Lu_{0\cdot2}$ specimen at 77 K. The bubble-shaped irreversible region centred near -2 Oe can be identified.

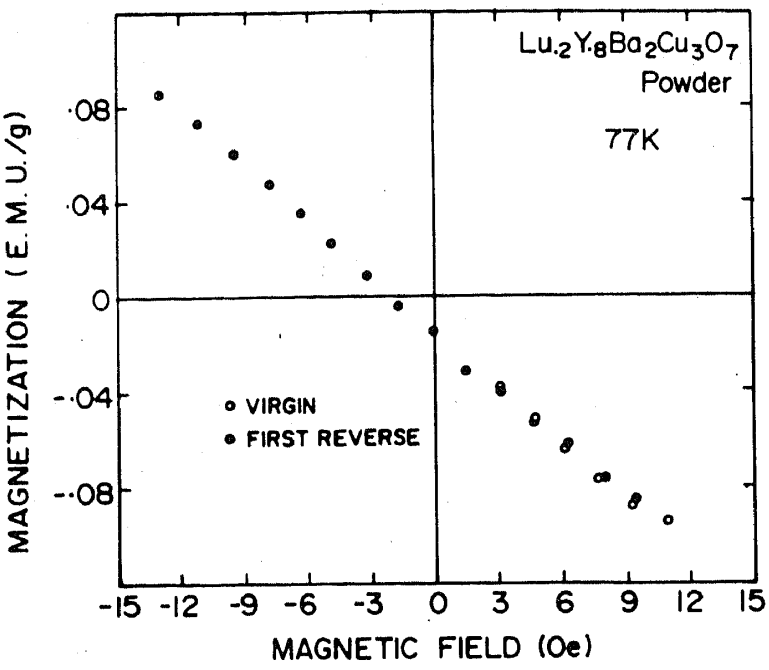

Figure 7. Magnetization vs field in ± 45 Oe at 77 K (after zero field cooling) for $Lu_{0.2}$ powdered specimen.

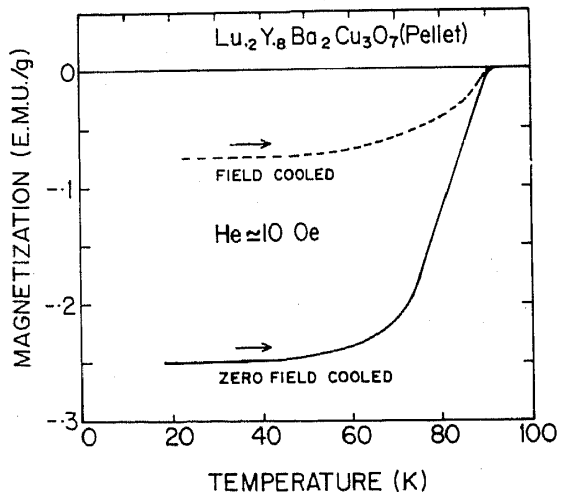

Figure 8. Temperature variation of ZFC and FC magnetization in a field of 10 Oe for sintered $Lu_{0.2}$ pellet. The arrows indicate that the data were recorded during warm-up from about 20 K.

3. Results

3.1 *Magnetic behaviour in DC fields*

The following features are noteworthy from the data presented in figures 1 to 8.

(i) There is a general resemblance in the magnetization response of sintered pellet and the crushed powder (see their major hysteresis curves in figures 1a and 6a for comparison at 77 K). The virgin M vs H_e plots are apparently linear upto about 100 Oe in both the cases and the initial slope values and the field values at which the magnetization turns over are nearly the same. The minimum magnetization value at the turnover point in the case of powder is less than, but within, 15% of that of the pellet.

(ii) A sharp dip in magnetization value is observed near $H_e = 0$ in the first reverse cycle at 77 K in the case of the pellet (see figure 1a). The anomalous jumps in magnetization values near $H_e = 0$ get more pronounced as the field is further cycled between ± 45 Oe (see figure 1b). These jumps near $H_e = 0$ seem to be superimposed on the minor hysteresis loop traced in ± 45 Oe. The curves corresponding to II forward and II reverse cycles in figure 1b constitute the minor hysteresis. No unusual change in magnetization values near $H_e = 0$ is perceptible (figure 6a) in the first reverse cycle in the case of powdered sample. However, an anomalous variation in magnetization values near $H_e = 0$ becomes somewhat perceptible as the field is reversed from -45 Oe to $+10$ Oe. Figure 6b shows the data during the second forward and second reverse cycles. As the field is cycled several times between ± 10 Oe, the shape of the magnetization curve stabilizes, as is evident from figure 6c. This figure shows an anomalous dip (or rise) in magnetization values near $H_e = 0$ and at higher fields the magnetization seems reversible within the scatter in our experimental data. The small minor hysteresis loop of figure 6c is centred around a nominal field value of -2 Oe instead of 0 Oe. This, as mentioned earlier, is due to the experimental error in absolute field values. The width of the region of the anomalous dip (and rise) for powder as well as the pellet (cf. figures 2b and 6c) appear to be of the same order as the smallest step (1·6 Oe) in which the DC field could be incremented. The height of the anomaly, i.e., the abrupt change in magnetization near $H_e = 0$, in the pellet is about one order of magnitude higher than that in the powder. The anomaly in the powder is above the scatter in our experimental data.

(iii) The comparison of data contained in figures 2 and 7 focusses attention onto an essential difference between the magnetic behaviour of pellet and powder in small fields. These figures show the response in the two cases in a field of $+10$ Oe after zero field cooling the specimens to 77 K. The virgin M vs H_e curves upto $+10$ Oe for both of them look similar, the initial slope value for powder being somewhat lower than that for the pellet. However, on reversing the field, a large flux is trapped (figure 2a) in the case of pellet whereas magnetization appears reversible (figure 7) within the sensitivity limit in the case of powder. In addition to the trapped flux, figure 2b shows the presence of anomalous kinks near $H_e = 0$ for pellet. The changes in magnetization values giving rise to the kinks in figure 2b, are about ten times smaller than in figure 1b, where the same sample had been exposed to large fields before cycling the field near the origin. We believe that the corresponding kinks in powder are perhaps buried within the scatter in the data of figure 7.

(iv) A comparison of figures 2b and 3 shows the change in the steady state response of

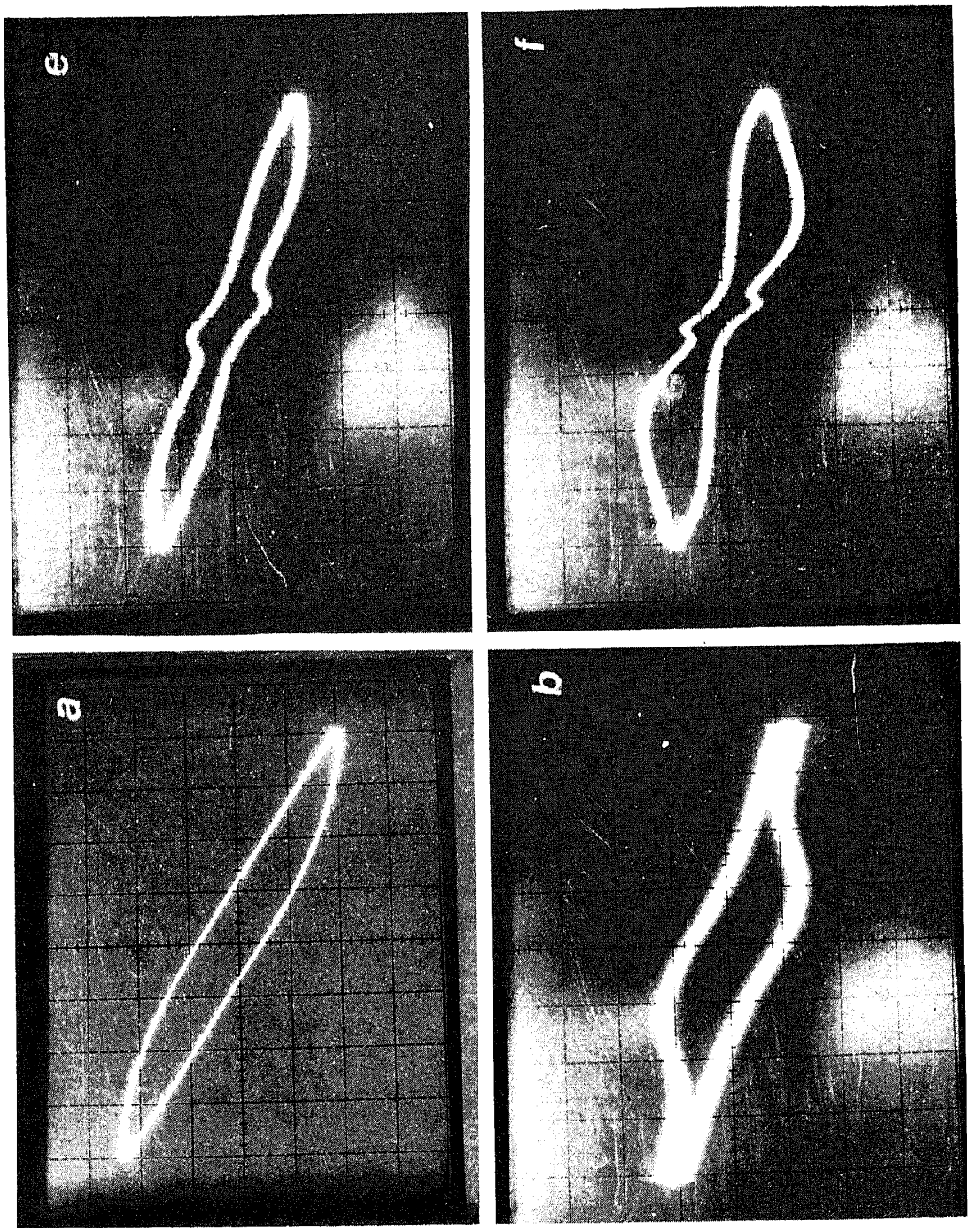
e
f
a
b

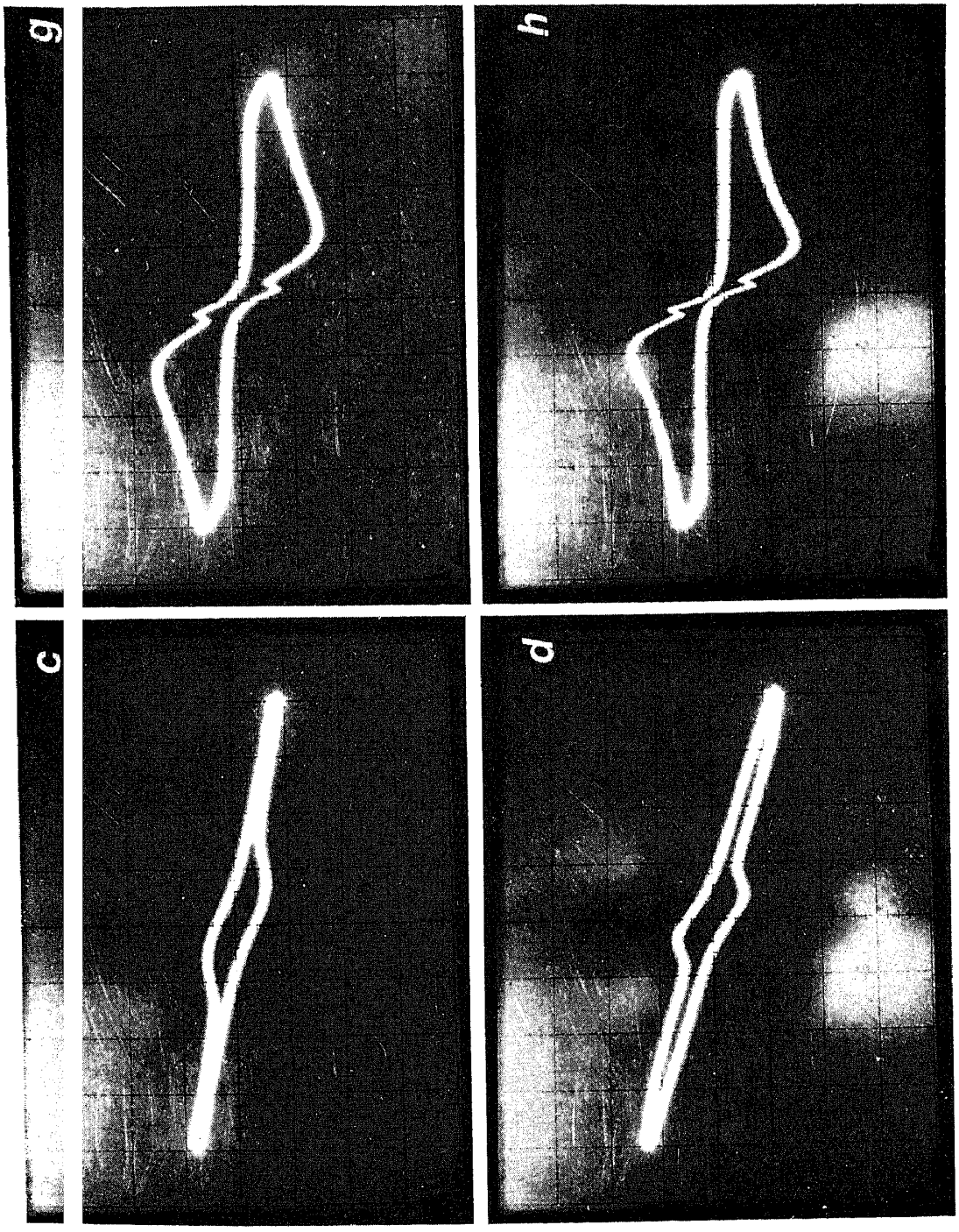

Figure 9. AC magnetic hysteresis loops at 77 K in different peak fields for sintered pellet of $Lu_{0.2}$. (**a**) 15 Oe, (**b**) 60 Oe, (**c**) 110 Oe, (**d**) 220 Oe, (**e**) 320 Oe, (**f**) 660 Oe, (**g**) 1080 Oe and (**h**) 1540 Oe. Vertical scale is arbitrary for all the loops.

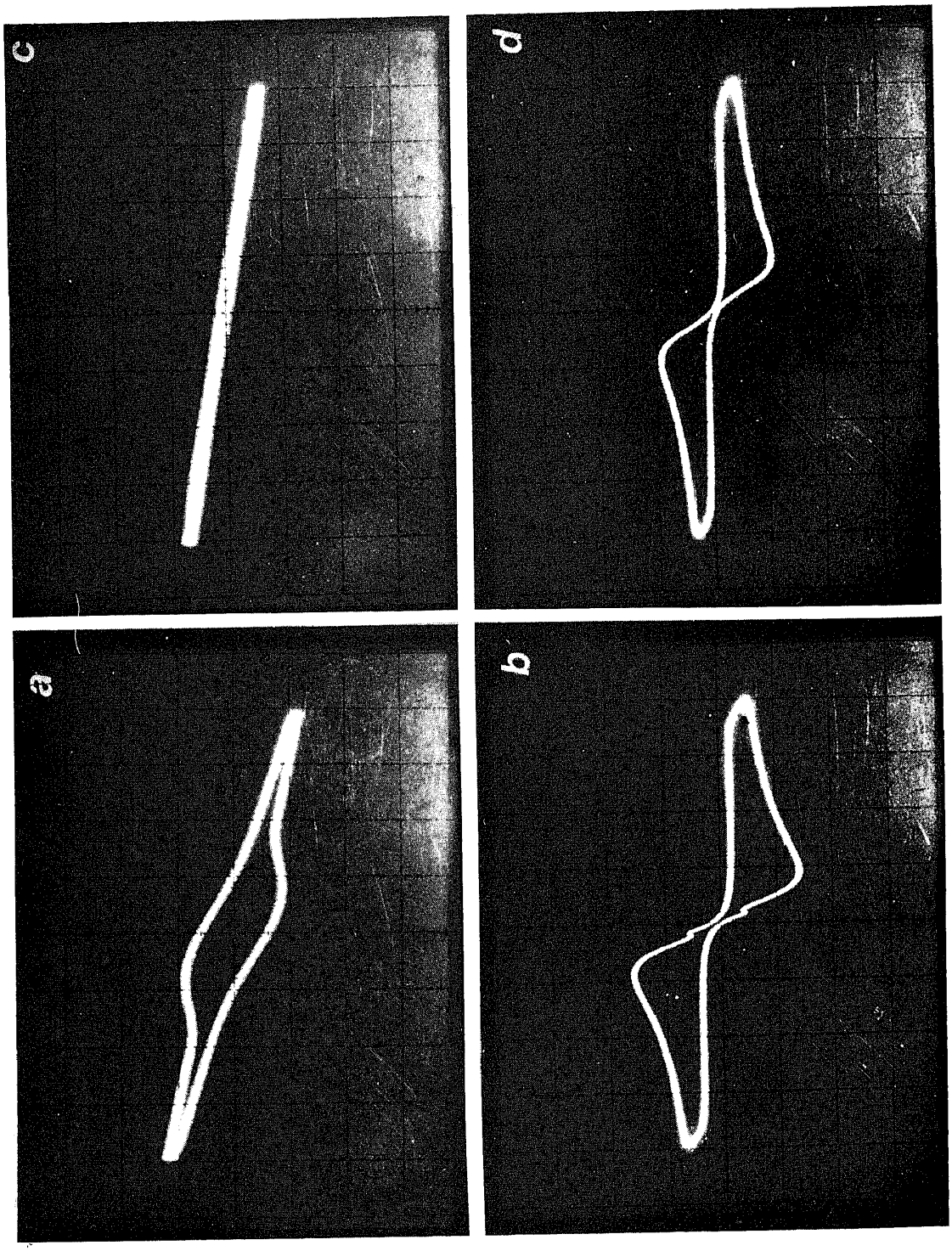

Figure 10. AC magnetic hysteresis loops at 77 K for sintered pellet (curves a and b) and powder (curves c and d) specimens of $Dy_{0\cdot2}Y_{0\cdot8}Ba_2Cu_3O_7$. Loops a and c are in peak field of 58 Oe whereas b and d are in peak field of 1520 Oe.

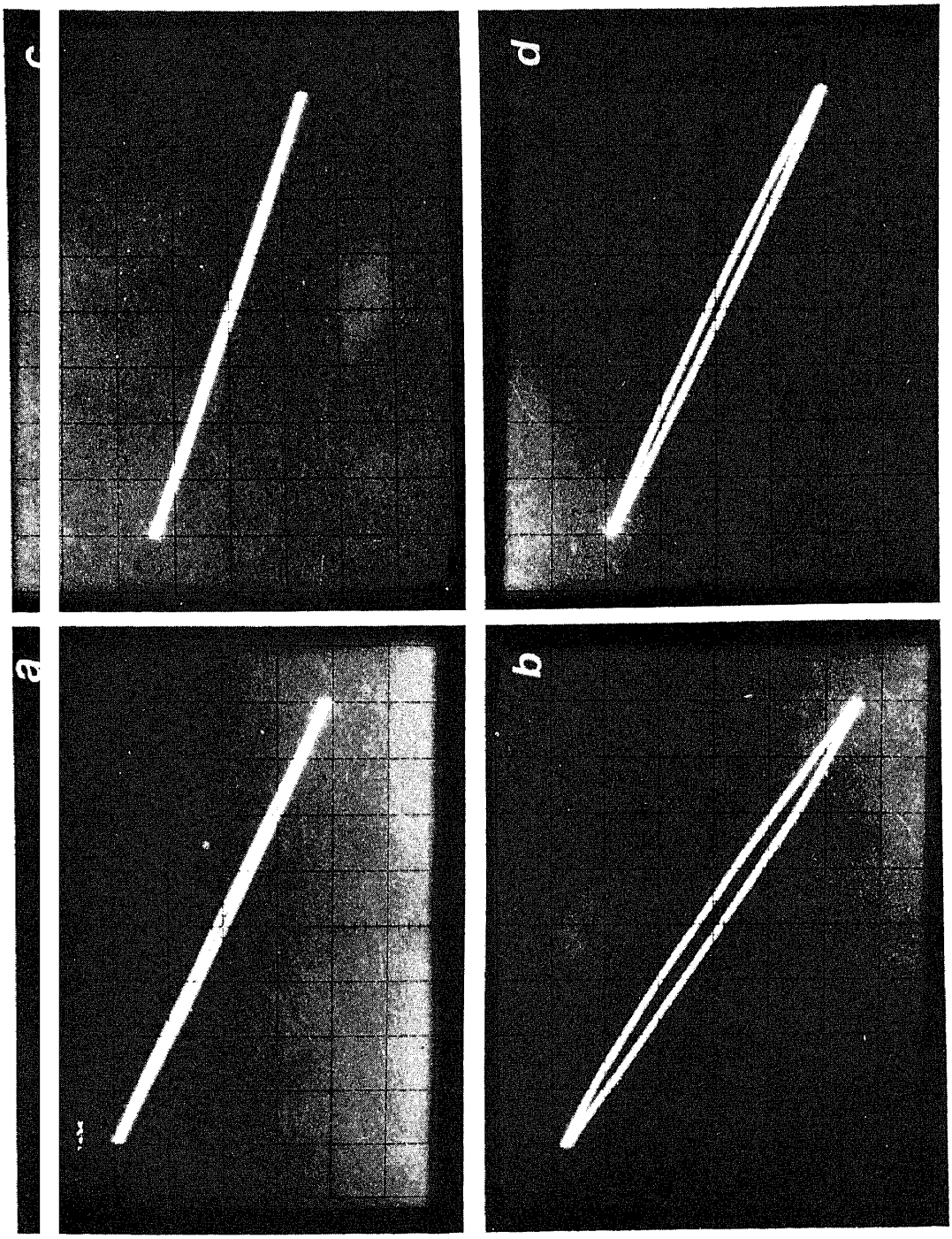

Figure 11. AC hysteresis loops at 77 K in peak fields of 5 Oe (a and c) and 8 Oe (b and d) for sintered pellet of $Lu_{0\cdot2}$ in two different orientations. In a and b the field was applied parallel to the cylindrical axis of the pellet whereas in c and d the field was in the plane of the pellet.

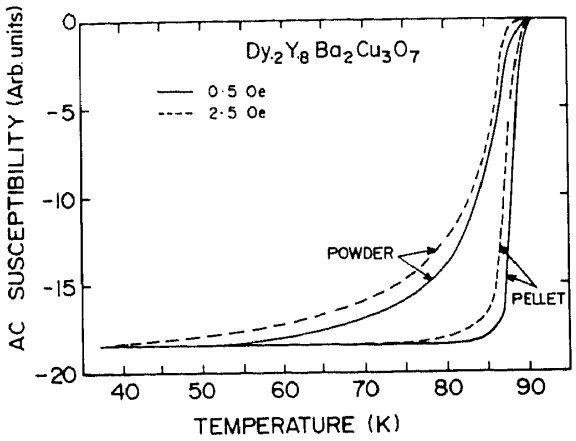

Figure 12. Temperature variation of ac susceptibility for sintered pellet and powdered specimens of $Dy_{0\cdot2}$ sample in two different values of peak field.

the pellet at 77 K as the maximum field, H_e, to which the specimen is cycled, is increased. After a certain threshold value of H_e (about 20 Oe in the case of the present specimen), the M vs H_e curve is linear and reversible within the scatter limit of the data. The slope of the linear portion at higher field values is not much different from the initial slope value during the virgin run. The hysteresis curve of figure 3, made up of reversible linear portion above a certain threshold superimposed on the irreversible bubble-shaped plot centred around the origin, is reminiscent of the plots reported by others (Senoussi *et al* 1987b, c; Renker *et al* 1987; Rosenberg *et al* 1987; Wiesniewski *et al* 1988) in the sintered pellet specimens of the two families of oxide superconductors. An additional feature evident in our present data, is the presence of anomalous kink(s) near $H_e = 0$. The irreversibility responsible for the bubble disappears in the case of powder. This is analogous to the absence of a bubble-like feature in the data of single crystal specimen of Senoussi *et al* (1987a).

(v) Figures 4 and 5 show the changes in the magnetic behaviour as the pellet is cooled down from 77 to 5 K. The major hysteresis loop (figure 4a) shows that the virgin M vs H_e plot is apparently linear up to about 500 Oe. The maximum value of magnetization during the virgin run and field value at which it occurs increases by a factor of ten at 5 K as compared to their corresponding values at 77 K (cf. figures 1a and 4a). On the reverse cycle, as the external applied field approaches zero value, the magnetization values rapidly drop from positive to negative values (see figure 4b for M vs H_e data on an expanded scale). As the field moves away from $H_e = 0$, the magnetization again increases as evidenced by open circle data points in figure 4b. On reversal of the field from about -45 Oe, the magnetization values retrace their path as H_e approaches zero value. As the field values move across $H_e = 0$, the magnetization swings back from negative to positive values. The behaviour depicted in figure 4b confirms the trend anticipated from the earlier report of scanty data in two types of high T_c superconductors (Grover 1988). The absolute height of the magnetization anomaly at 5 K is more than ten times that at 77 K, whereas the width is of the same order (cf. figures 1b and 4b). Figure 5 shows that even at 5 K, the height of the anomaly decreases if the specimen is not exposed to a high field before the reversal of the field. This is similar to the trend evident from the comparison of data in figures 1b and 2b. The threshold field

alue up to which magnetization remains irreversible near the origin also appears to be igher at 5 K as compared to that at 77 K (cf. figures 2a, 4 and 5).

(vi) Figure 8 shows the comparison of magnetization behaviour in ZFC and FC tates of pellet. The magnetization has been measured in a nominal field of 10 Oe which s much larger than the field value corresponding to the width of the anomaly near $H_e = 0$, as discussed above. The ZFC and FC magnetization values appear saturated below about 50 K. The saturated ZFC magnetization corresponds to $4\pi M/H$ value of about $\pi\rho/10$, where $\rho(= 5{\cdot}1$ g/cc) is the physical density of the pellet. This value of about ·6 for $4\pi M/H$ is consistent with another independent estimate for this factor obtainable from the slope of the initial linear portion of virgin M as H_e curve at 5 K in igure 5.

3.2 *Magnetic behaviour in AC fields*

The important points emerging from the AC magnetization studies are as follows:

(i) There is a close correspondence between the DC and AC magnetic response of the same specimen. This is evident from a comparison of figures 2a and 3 with figures 9a and b respectively and of figure 1a with the relevant portion of hysteresis curve of igure 9h for the specimen of $Lu_{0{\cdot}2}Y_{0{\cdot}8}Ba_2Cu_3O_7$. The virgin M vs H_e curve cannot be seen in the AC plots. The shape of the magnetic hysteresis curves generated on repeated cyclings in DC fields are similar to those of the AC hysteresis loops.

(ii) The anomalous kinks centred at $H_e = 0$ in DC data (figures 2b and 3) are not perceptible in the corresponding AC data. The pair of kinks visible in the AC hysteresis loops (figures 9e to h) do not correspond to the kinks in DC data. The kinks in figure 9 are located in the second ($H_e < 0$) and fourth quadrant ($H_e > 0$) instead of being centred at $H_e = 0$, as in the DC data. The anomalous kinks in the AC hysteresis loops are a manifestation of irreversible response in low fields. This fact is well evident from an examination of the change in the shape of the loops depicted in figures 9a to h, as the peak field increases. The bubble-like minor hysteresis loop in low fields (figures 9a to c) appears as a pair of kinks in major hysteresis loops (figures 9f to h). The bubble-shaped hysteresis regions are evident (figures 2b and 3) in low DC fields as well, but the corresponding kinks are not visible in our high field DC data (figure 1a) as we could not reverse the DC field below about -50 Oe on our set-up. Figure 9h shows that the kink is located beyond this field value. However, the loop formed by II forward and II reverse cycles in the DC data of figure 1b clearly shows the presence of bubble-like irreversible region extending between about ± 45 Oe. The shape of the bubble in figure 1b appears distorted near $H_e = 0$ due to the superposition of anomalous jumps in this region. The DC data, therefore, at least display all the features contained in the AC hysteresis curves; however, the converse need not be true due to the limitations in the sensitivity and the time resolution factor in AC techniques.

(iii) There exists a direct correlation between the relative prominence of the anomalous kinks in the high field AC hysteresis loops and the width and the area of the minor hysteresis loops observable in low fields. For the $R_{0{\cdot}2}Y_{0{\cdot}8}Ba_2Cu_3O_7$ series of specimens studied by us, the prominence of the kinks decreases in the order, $Lu_{0{\cdot}2}$ $Ho_{0{\cdot}2}$, $Dy_{0{\cdot}2}$, $Yb_{0{\cdot}2}$, $Gd_{0{\cdot}2}$.

(iv) A variation is observed in the low field response (minor loops) amongst different sintered pellets with the same nominal chemical composition. Correspondingly, the differences are also observed in the prominence of the kinks in their high field AC

hysteresis loops. On powdering a given sintered pellet, the irreversibility (bubble-shaped region) in its minor AC hysteresis loop and the corresponding kinks in its major AC hysteresis loop disappear. Besides the kinks, there is not much difference in the general shape of the high field AC hysteresis loops of sintered pellet and the powdered form of the same specimen at the same temperature. One of the powdered specimens was compacted, into a pellet at room temperature and its AC hysteresis response was studied. No difference was observed in the response of this unsintered (cold) pellet and its powdered form.

(v) Another important feature evident from the sequence of loops depicted in figures 9e to h is that the magnitude of maximum magnetization and the field values corresponding to this magnetization are nearly independent of the peak field in which the sample is cycled. The same trend is observed in the data of all the compounds, however, the actual values differ in different samples.

(vi) Figure 11 shows minor hysteresis loops in peak fields of 5 Oe (figures 11a and c) and 8 Oe (figures 11b and d) applied parallel and perpendicular to the cylindrical axis of the sintered pellet of $Lu_{0.2}$ specimen (diameter = 7·8 mm and thickness = 2·2 mm). In a field of 5 Oe the loop is slightly open (figure 11a) when the field is parallel to the cylindrical axis, whereas it appears closed when perpendicular to the axis (figure 11c). The difference in behaviour observed for two different orientations is due to the difference in the demagnetization factors. Because of the porus nature of sintered pellets, the demagnetization factor for these specimens cannot be reliably calculated and will be smaller than that ascertained from their geometrical shape and the relative orientation of the applied field. However, a good estimate can be made by measuring the threshold field values at which the irreversibility is visible (as in figure 11a) in three orthogonal directions for a given specimen. The trace of the demagnetization tensor equals unity. Therefore if n is the demagnetization factor for a field applied parallel to the cylindrical axis of the pellet and x is the ratio of the threshold fields in parallel and perpendicular directions to the axis, then it is easy to show that $n = (2 - x)/(2 + x)$. We could estimate the values of n from the low field hysteresis data of the kind shown in figure 11 in all the specimens. These estimated values were considerably lower than the values calculated from the geometrical considerations alone. For $Lu_{0.2}$ specimen, n is found to be $0{\cdot}45 \pm 0{\cdot}05$ as compared to a value of $0{\cdot}65 \pm 0{\cdot}05$ determined from its shape and size assuming solid density.

(vii) Figure 12 shows the comparison of temperature variation of AC susceptibility for sintered pellet and powder form of $Dy_{0.2}Y_{0.8}Ba_2Cu_3O_7$ in peak fields of 0·5 and 2·5 Oe. The samples were cooled down to 20 K in nominal zero field and measurements were made during warm up cycles. The saturated value of AC susceptibility in a field of 0·5 Oe for powder form is normalized to the saturated value of the pellet. The data in figure 12 show that the width of the transition increases considerably on powdering. The increase in amplitude of the AC field from 0·5 to 2·5 Oe broadens the width of the transition seen for the pellet as well as for the powder. It may be noted that no significant change takes place in the value of superconducting transition temperature, as identified by the onset of dimagnetic response, on powdering a sintered pellet.

4. Theoretical considerations on magnetization curves

Bean (1962, 1964) formulated a model for the hysteretic behaviour of hard superconductors and this has been tested over the years (Campbell and Evetts 1972). We

shall first outline Bean's model and then briefly discuss its extension for high T_c superconductors (Ravi Kumar and Chaddah 1987, 1988).

4.1 *Bean's model*

Bean considered the virgin magnetization for finite (Bean 1962) and zero (Bean 1964) H_{c1} and the hysteresis curve only for zero H_{c1}. The virgin curve shows complete flux expulsion for $H_e < H_{c1}$, but for $H_e > H_{c1}$ the shielding currents are set up which have a magnitude J_c and flow in a field-dependent penetration depth. If we make an assumption that H_{c1} is negligible, then the virgin magnetization curve is determined solely by the shielding currents and is given by (Bean 1964)

$$M = -H + H^2/kH^*, \tag{1}$$

where $H^* = \mu_0 J_c D/2$ and $k = 2$ for an infinite slab of width D with field parallel to the surface. This is plotted in figure 13 for $H^* = 0{\cdot}63\ T$ and compared with the case of complete flux expulsion.

4.2 *Present model*

4.2a $H_{c1} = 0$ *case.* Based on experimental data (see e.g. Farrell *et al* 1987; Senoussi *et al* 1987a) on high T_c superconductors, Ravi Kumar and Chaddah (1987) extended Bean's model. While Bean assumed that J_c is independent of field, they assumed that

$$J_c(H) = J_c(0)\exp(-H/H_0). \tag{4.2}$$

The calculated virgin magnetization curve is also shown in figure 13 and two features stand out in contrast to the results of Bean. Firstly the magnetization does not saturate at high fields and this results in hysteresis curves whose shape changes qualitatively as the maximum applied field is changed. Secondly there is a peak in the magnetization curve and the field corresponding to this turnover point is sometimes (see e.g. Maletta *et al* 1987) confused with H_{c1}.

4.2b *Non zero* H_{c1}. For a non-zero but small (compared to H^*) H_{c1} there will be no experimentally perceptible change in the virgin magnetization curve. An interesting

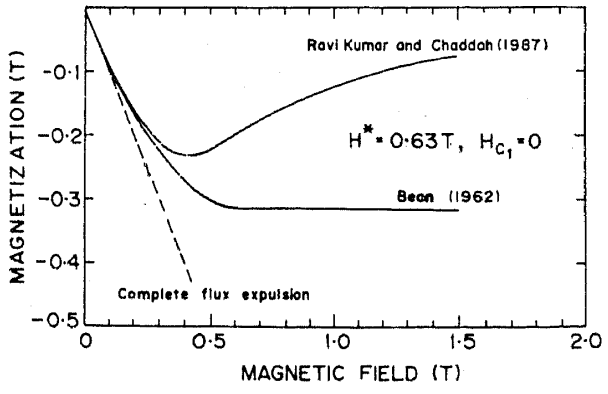

Figure 13. Virgin magnetization curves calculated in the framework of Bean (1962) and Ravi Kumar and Chaddah (1987). The dotted line corresponds to complete flux expulsion.

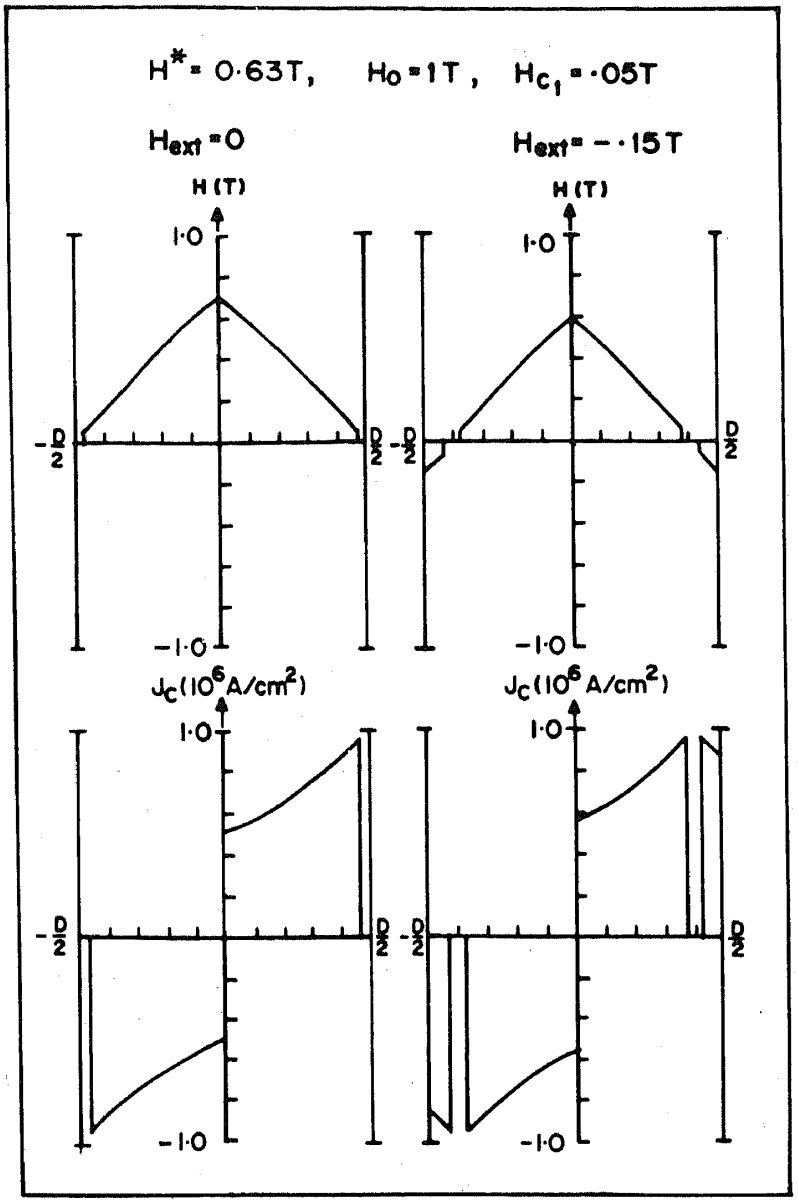

Figure 14. Field and current density distributions at two different values of externally applied field in an infinite slab of width D in the framework of model calculations (see text). The applied field is cycled upto $3T$ before reversal. The values of the other parameters of the model are indicated in the figure.

anomaly is predicted, however, in the hysteresis curve near $H = 0$. The anomaly is best understood by considering figure 14 where we show the remanent field distribution and the macroscopic current distribution in a hysteretic sample. When the external field is zero, the region near the surface sees a field below H_{c1} and, following Bean (1962), is shielded by the "soft" superconductor and the macroscopic current density is reduced to zero. We refer to this region as the "Meissner zone". Compared to the case of $H_{c1} = 0$, the magnetization contribution from the Meissner zone consists of two different terms.

These are

$$\Delta M = -1/D \int H(x)\,dx - \mu_0/D \int J(x)x\,dx, \tag{3}$$

where the domain of integration is the Meissner zone. For $H_{c1} \ll H^*$, the first term is small and shall be ignored for the present discussion. The Meissner zone starts forming at $H = +H_{c1}$, and continues to grow in size till $H = -H_{c1}$ and in this region the second term and thus ΔM grows in magnitude. As the applied field is reversed below $-H_{c1}$ the Meissner zone stops growing in size and moves inwards and this is depicted in figure 14. Because of the weight factor in the integrand, the contribution of the second term and thus the magnitude of ΔM drops. The anomaly thus extends from $+H_{c1}$ to $-H_{c1}$ and is discussed in detail by Ravi Kumar and Chaddah (1988). Following their prescription, we present in figure 15, qualitative changes in the shape of the hysteresis curves and the manifestation of the anomaly as the maximum applied field is varied. We also state that the height of the anomaly increases with increasing maximum applied field.

Figure 15d shows that magnetization peaks at a field H_{peak}. For a given H^*, H_{peak} is independent of the maximum field H_{max}. Figure 15a shows that for H_{max} slightly greater than H_{c1} the hysteresis loop appears to be made up of an irreversible bubble region

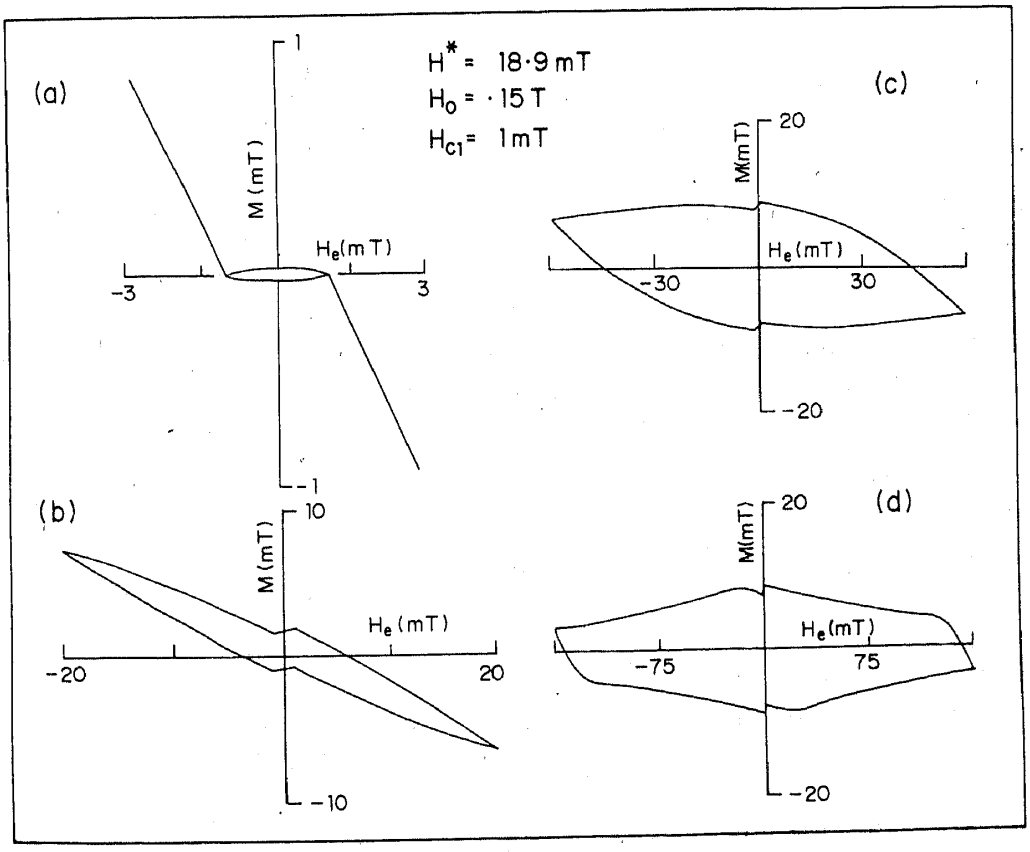

Figure 15. Calculated magnetic hysteresis loops for different values of H_e^{max} in which the cyclings are done. The values of other parameters are $H^* = 18{\cdot}9$ mT, $H_0 = 0{\cdot}15$ T and $H_{c1} = 1$ mT.

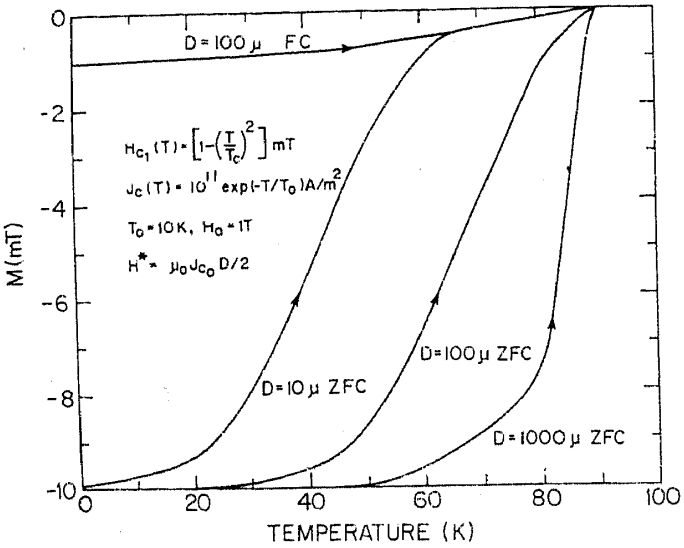

Figure 16. Calculated curves for the temperature variation of ZFC and FC magnetization in externally applied magnetic field of 10 mT. The curves are labelled by the thickness of an infinite slab. The values of other parameters in the model are shown in the figure.

between $+H_{c1}$ and $-H_{c1}$ surrounded on both sides by apparently reversible wings. The anomalous kinks (figures 15b to d) centred at $H_e = 0$ are a consequence of finite H_{c1}. The height of the anomaly grows in magnitude as H_{max} is increased.

4.3 *Field cooled and zero field cooled magnetization*

A type II superconductor, when cooled below T_c in a magnetic field $H > H_{c1}$, goes into a mixed state with a magnetization $M(H)$, where $M(H)$ is less than H_{c1} and $M(H)$ falls to zero as H approaches H_{c2}. However, if a magnetic field $H > H_{c1}$ is applied to a superconductor after cooling it below T_c in a zero field, shielding currents are set up which give rise to magnetization. It is easy to argue that for $H_{c1} < H \ll H^*$, the ZFC sample will always show a larger magnetization than the FC sample. We have calculated FC magnetization values as a function of temperature assuming that

$$M(H, T) = -H_{c1}(T) \quad \text{for } H_{c1} < H \ll H_{c2}. \tag{4}$$

For calculating the ZFC magnetization we have also assumed a temperature dependence in J_c such that

$$J_c(H, T) = J_{c0}\exp(-T/T_0)\exp(-H/H_0). \tag{5}$$

In figure 16 the calculated FC and ZFC curves have been shown. It is evident that as the size of the particles is reduced, the width of the transition increases for the ZFC case.

5. Discussion

The results of the model calculation of virgin magnetization and hysteresis curves and of the temperature dependence of magnetization presented in the previous section were

for an infinite slab geometry of the sample. Besides computational ease, there are no demagnetization corrections in this geometry. The experimental results presented in § 3 are on sintered pellets and powders. While the latter could be approximated to a spherical geometry, the former are of less than 80% solid density and no satisfactory geometrical approximation of the shape is possible. In view of the difference in the sample shape from that used in the calculations and the complexity in computation for shapes other than an infinite slab, we shall make only qualitative comparisons between the experimental data and the results of the model calculations.

5.1 *Magnetic isotherms*

Sintered pellets consist of superconducting grains coupled by intergranular links whereas a powdered specimen (or a cold pellet) consists of decoupled grains. It is for this reason that only the sintered pellets show zero resistance, while the diamagnetic response of both samples signifies the intrinsic (intragranular) superconducting state. The transport critical current of a sintered pellet is much smaller than that of either a single crystal or a single grain (intrinsic) since it is determined by the intergranular links. It is clear from our dc data that the common features in the magnetic behaviour of the sintered pellet and the powdered specimens arise from the superconducting grains whereas features like the low field hysteresis originate from the screening currents flowing across the intergranular links. An additional evidence in favour of the hypothesis that the low field hysteresis arises from intergranular region comes from the correlation between the measured values of transport current densities at 77 K in a series of $Y_{0\cdot8}R_{0\cdot2}Ba_2Cu_3O_7$ specimens and the width and the area of the minor hysteresis loops in them. The current densities in $Dy_{0\cdot2}$, $Yb_{0\cdot2}$ and $Gd_{0\cdot2}$ specimens are measured (P K Mishra, private communication) to be 55, 40 and 20 A/cm^2 respectively at 77 K, and the observed trend is consistent with the decreasing width and area of the minor hysteresis loops in them (see § 3).

It has been argued by Clem and Kogan (1987) that the lower critical field values of the intergranular links are extremely low (< 20 mOe). Therefore when a sintered pellet is exposed to an applied field, the screening currents at a density equal to the intergrain critical current density, J_c^{pel}, are set up in the pellet in the same way as described in § 4. The magnetization curves resulting from these supercurrents are similar in nature to the Bean's curves (Bean 1964). However, if we incorporate the field dependence of J_c^{pel} (see e.g. Noto *et al* 1987), the hysteresis curves similar to that depicted in figures 15b to d will result. The maximum value of magnetization and the width (i.e., the region of irreversibility) of the loop are both expected to be determined by the H^* value of the pellet. For the pellet, $H^* = \mu_0 J_c^{pel} d/2$, where d is the dimension of the pellet normal to the field direction. In the case of $Dy_{0\cdot2}$ specimen ($d = 7{\cdot}8$ mm), $H^* \sim 25$ Oe at 77 K. Such an estimate appears to be qualitatively consistent with the width of its minor hysteresis loop depicted in figure 10a.

As the applied field is increased very much beyond the H^* value of the pellet, the applied field virtually penetrates the intergranular region and the magnetic behaviour of the pellet starts to get governed by the H^* value of the grains. The shielding currents flowing inside the grain (or a single crystal) have much higher densities ($\sim 10^6$ A/cm^2 at 77 K) and the corresponding H^* value is $0{\cdot}05\ T$ for a grain of size 10 microns and consequently we observe a reversible region beyond the low field bubble. In the case of powdered specimens the magnetic behaviour is governed by this large H^* value of the

grain even in the low field region during the virgin run. This explains the absence of the low field hysteretic bubble in the case of powdered sample (figure 10c).

The general features of magnetization curves (ignoring the bubble-shaped irreversible region centred at the origin due to intergranular links) depicted in figure 9, can now be understood in terms of the results of model calculations, with typical H^* values of the grain. The observed changes in the shape of magnetization curves shown in figures 9e to h can be easily identified with calculated shapes in figures 15b to d. The field value (250 Oe) corresponding to the maxima in magnetization remains unchanged in figures 9e to h. This value is about the same at which the DC magnetization peaks during the virgin runs at 77 K in pellet and powder specimens as shown in figure 1a and figure 6a respectively. In the framework of model calculations (see Ravi Kumar and Chaddah 1987) this field value must be less than the H^* value of the superconducting grain. An estimate of lower limit of 250 Oe for H^* value at 77 K is qualitatively consistent with the typical grain dimensions (~ 10 microns) and the observed values of current densities ($\sim 10^6$ A/cm^2) at 77 K in single crystal specimens of $RBa_2Cu_3O_7$ family. It may also be mentioned here that the above values for the dimensions of the grain and the critical current densities in them are also consistent in the framework of Bean's model with the DC magnetization values shown in figures 1a and 6a.

As discussed in § 4 the anomalies centred at the origin in the magnetic hysteresis loops shown in figure 15 are a manifestation of the lower critical field. The anomaly depicted in figures 15b to d may be identified with the observed kinks near $H_e = 0$ in figures 1 to 6. In the case of sintered pellet (figures 2, 3 and 5) the observed anomalous kinks near $H_e = 0$ appear superimposed on minor hysteresis loop due to intergrain supercurrents. Figure 6b shows that the minor hysteresis loop collapses in the powder specimen whereas the anomalous kinks survive. It may be recalled here that similar kinks are visible in the high field magnetic hysteresis data at 5 K of single crystal specimen of $HoBa_2Cu_3O_7$ (Schneemeyer *et al* 1987). We believe that our powder specimen consisting of randomly oriented grains emulates the behaviour seen in single crystal specimens. We identify the calculated hysteresis curve of figure 15a with the observed hysteresis loop shown in figure 6c. The latter has been obtained after first exposing the specimen to high field values (> 1 kOe), whereas the calculated curve is obtained only by cycling the specimen within 30 Oe. As described in § 3.1, we observed that the exposure of the virgin specimen to high fields enhances the height of the anomalous kink. In the absence of this exposure (see figure 7) the anomaly is perhaps buried within the scatter limit of our data. The width of the anomaly in figure 6c is of the same order as the smallest step in which we could increment the DC field. Thus our estimate of lower critical field from figure 6b in superconducting grains of $Lu_{0.2}Y_{0.8}Ba_2Cu_3O_7$ is limited to a value of < 2 Oe at 77 K.

5.2 *Temperature variation of magnetization*

The observed difference in the temperature variation of diamagnetic response in pellet and powder specimens of $Dy_{0.2}Y_{0.8}Ba_2Cu_3O_7$, as depicted in figure 12, can be understood in terms of grain size effects as shown in figure 16. On crushing a given pellet the average size of the grains is expected to decrease, and consequently the diamagnetic response decreases. Figure 12 also shows that the difference in ac susceptibility values obtained in fields of 0·5 and 2·5 Oe in powder specimen persists down to about 40 K. As stated in § 4.2, this implies that $H_{c1} < 2{\cdot}5$ Oe for $T > 40$ K in this specimen.

Figure 8 shows the temperature variation of ZFC and FC magnetization in a sintered pellets specimen of $Lu_{0\cdot2}Y_{0\cdot8}Ba_2Cu_3O_7$ in an applied DC field of 10 Oe. The width of the magnetization anomaly at 5 K in the same specimen (see figures 4 and 5) is much less than 10 Oe. Thus the ZFC and FC magnetization data of figure 8 have been obtained in a field value larger than the expected $H_{c1}(0)$ value. The observed difference in ZFC and FC magnetization curves is, therefore, qualitatively consistent with the results of model calculations shown in figure 16 (for grains of size 100 microns) where the measuring field is larger than $H_{c1}(0)$. We note that the calculated values of ZFC magnetization saturate at low temperatures and correspond to nearly complete flux expulsion. The measured values of ZFC magnetization have to be corrected for the demagnetization factor. Assuming that our zero field magnetization values at low temperatures (see figures 5 and 8 and § 3.2) correspond to complete flux expulsion, we get a value of about 0·38 for the demagnetization factor for a cylinder of length 2·2 mm and diameter 6·5 mm. This value of 0·38 is to be compared with a value of about 0·55 obtained from geometrical considerations alone. The difference between these two values is consistent with the analysis presented in § 3.2 for such a sintered pellet.

5.3 *Comments on existing data*

We have argued above that our data on various $RBa_2Cu_3O_7$ samples imply H_{c1} values of a few Oe. We shall now discuss two sets of data often quoted in the oxide superconductors that also lead to similar conclusions.

We first discuss the high accuracy ZFC and FC data of Maletta *et al* (1987) on $La_{1\cdot8}Sr_{0\cdot2}CuO_4$. They measure susceptibility on ZFC samples in fields varying from 0·01 Oe to 100 Oe, and find that the flux expulsion is never complete. Further susceptibility is independent of field till 1 Oe, and drops at 1 Oe $< H_e <$ 10 Oe. This is consistent with our estimate of H_{c1}. For $H_e < H_{c1}$, the screening current flows only in the London penetration depth, and flux expulsion is not complete for finite size samples (Clem and Kogan 1987). Susceptibility is, however, independent of H_e in this regime. For $H_e > H_{c1}$ the shielding currents flow deeper inside the sample, and susceptibility decreases with increasing H_e. The data of Maletta *et al* thus clearly show that H_{c1} lies between 1 Oe and 10 Oe. We also show in figure 17 the virgin magnetization curve obtained by Maletta *et al*, its qualitative agreement with our model, for $H_{c1} = 0$ is apparent on comparison with figure 13.

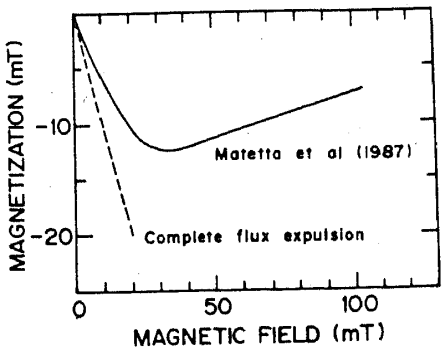

Figure 17. Virgin magnetization curve obtained for a sintered pellet specimen of $La_{1\cdot85}Sr_{0\cdot15}CuO_4$ by Maletta *et al* (1987). The dotted line corresponds to complete flux expulsion.

Our low value of H_{c1} is also consistent with the results of Gammel *et al* (1987) on single crystal $YBa_2Cu_3O_7$. They see an ordered vortex lattice at 4·2 K even when the sample is cooled in a field of 13 Oe. They also see such a lattice in fields of about 30 Oe, 50 Oe, 110 Oe and 170 Oe. The lattice spacing of the vortex structure scales inversely as the square root of the field in which the sample is cooled. The lattice cannot be ascribed to flux vortices pinned to inhomogeneities as inhomogeneities spaced so appropriately would be extremely fortuitous. It is thus clear that the sample studied by Gammel *et al* has $H_{c1} < 13$ Oe at 4·2 K.

In this section we have established the qualitative agreement of our data with the model of Ravi Kumar and Chaddah that current densities in high T_c superconductors decay sharply with field. We have shown that our results are characteristic of intrinsic, intragranular superconductors. We find that H_{c1} values of the high T_c superconductors are extremely low.

6. Summary and conclusions

We have presented magnetization data on $RBa_2Cu_3O_7$ family of superconductors. Comparison of data on sintered pellets and powdered samples has helped identify the features that are intrinsic to these compounds and originate from the intragrain region and those which emanate from the intergranular links. We have established consistency between magnetization data obtained by DC and low frequency AC methods. The isothermal AC and DC data, and the temperature variation of magnetization of ZFC and FC states of the specimen are all in good agreement with the values calculated following the prescription of Ravi Kumar and Chaddah (1987) to extend Bean's (1962) model.

We have observed two kinds of anomalies in the magnetic hysteresis curves. One pair of anomalies are located away from the $H_e = 0$ line and this is a feature of the intergranular links. The field at which this pair of anomalies occurs correlates well with the transport critical current density of the sintered pellet. The other set of anomalies is centred about the $H_e = 0$ line and is consistent with the prediction of Ravi Kumar and Chaddah (1987). We have shown that these anomalies are intrinsic to the high T_c compounds. This set of anomalies, which are also evident in the magnetic hysteresis data of single crystal specimen (Schneemeyer *et al* 1987), imply H_{c1} values of about a few Oe. We show that this is also consistent with other published data (Maletta *et al* 1987; Gammel *et al* 1987), but in total disagreement with the large values of H_{c1}, often quoted (Dinger *et al* 1987; Crabtree *et al* 1987). Such low values of H_{c1} would, besides having implications for applications (Padamsee 1987), alter the presently quoted (e.g. Umezawa *et al* 1987b) microscopic parameters of these superconductors.

References

Bean C P 1962 *Phys. Rev. Lett.* **8** 250
Bean C P 1964 *Rev. Mod. Phys.* **36** 31
Campbell A M and Evetts J E 1972 *Adv. Phys.* **21** 199
Clem J R and Kogan V G 1987 *Jpn. J. Appl. Phys. Suppl.* **26** 1161
Crabtree G W, Lin J Z, Umezawa A, Kwok W K, Sowers C H, Malik S K, Veal B W, Lam D J, Brodsky M B and Downey J W 1987 *Phys. Rev.* **B36** 4021

Dinger T R, Worthington T K, Gallagher W J and Sandstrom R L 1987 *Phys. Rev. Lett.* **58** 2687
Farrell D E, Chandrasekhar B S, DeGuire M R, Fang M M, Kogan V G, Clem J R and Finnemore D K 1987 *Phys. Rev.* **B36** 4025
Gammel P L, Bishop D J, Dolan G J, Kwo J R, Murray C A, Schneemeyer L F and Waszczak J V 1987 *Phys. Rev. Lett.* **59** 2592
Grover A K 1988 (submitted)
Grover A K, Radhakrishnamurty C, Chaddah P, Ravi Kumar G and Subba Rao G V 1988 *Pramana – J. Phys.* **30** L167
Hammann J, Ocio M, Bertinotti A, Luzet D, Vincent E, Revcolevschi A and Jegoudez J 1987 (preprint)
Likhite S D and Radhakrishnamurty C 1966 *Curr. Sci.* **35** 534
Maletta H, Malozemoff A P, Cronemeyer D C, Tsuei C C, Greene R L, Bednorz J G and Mueller K A 1987 *Solid State Commun.* **62** 323
Marcus J, Escribe-Filippini C, Schlenker C, Buder R, Devenyi J and Reyder P L 1987 *Solid State Commun.* **63** 129
Noto K, Morita H, Watanabe K, Murakami Y, Obi Y, Fujimori H, Kobayashi N and Muto Y 1987 *Jpn. J. Appl. Phys. Suppl.* **26** 1195
Padamsee H 1987 (preprint)
Radhakrishnamurty C, Likhite S D and Sastry N P 1971 *Philos. Mag.* **23** 503
Ravi Kumar G and Chaddah P 1987 (submitted)
Ravi Kumar G and Chaddah P 1988 (submitted)
Renker B, Apfelstedt I, Kupfer H, Politis C, Rietschel H, Schauer W, Wuhl H, Gottwick U, Kneissel H, Rauchschwalbe U, Spille H and Steglich F 1987 *Z. Phys.* **B67** 1
Rosenberg M, Mittag M, Job R, Chojetzki W, Wernhardt R, Sabrowsky H and Neubauer R 1987 *Z. Phys.* **B69** 151
Schneemeyer L F, Gyorgy E M and Waszczak J V 1987 *Phys. Rev.* **B36** 8804
Senoussi S, Oussena M and Collin G 1987a (preprint)
Senoussi S, Oussena M, Ribault M and Collin G 1987b *Phys. Rev.* **B36** 4003
Senoussi S, Oussena M and Hadjoudj S 1987c *J. Appl. Phys.* (in press)
Subba Rao G V, Varadaraju U V, Thomas K A, Vijayashree R, Raju N P, Srinivasan R, De U, Janaki J and Radhakrishnan T S 1987 *Jpn. J. Appl. Phys. Suppl.* **26** 1077
Umezawa A, Crabtree G W, Liu J Z, Weber H W, Kwok W L, Nunez L H, Moran T J, Sowers C H and Claus H 1987a *Phys. Rev.* **B36** 7151
Umezawa A, Crabtree G W, Liu J Z, Moran T J, Malik S K, Nunez L H, Kwok W L and Sowers C H 1987b (preprint)
Wiesniewski A, Baran M, Przyslupski P, Szymczak H, Pajaczkowska A, Pytel B and Pytel K 1988 *Solid State Commun.* **65** 577